Mutation Research xxx (2015) xxx–xxx

Contents lists available at ScienceDirect

Mutation Research/Genetic Toxicology and Environmental Mutagenesis

journal homepage: www.elsevier.com/locate/gentox
Community address: www.elsevier.com/locate/mutres

Sub-micrometer 20 MeV protons or 45 MeV lithium spot irradiation enhances yields of dicentric chromosomes due to clustering of DNA double-strand breaks

T.E. Schmid[a,*,1], W. Friedland[b,1], C. Greubel[c,1], S. Girst[c], J. Reindl[c], C. Siebenwirth[a,c], K. Ilicic[a], E. Schmid[d], G. Multhoff[a], E. Schmitt[b], P. Kundrát[b], G. Dollinger[c]

[a] Department of Radiation Oncology, Technische Universität München, Germany
[b] Institute of Radiation Protection, Helmholtz Zentrum München—German Research Center for Environmental Health, Neuherberg, Germany
[c] Institute for Applied Physics and Metrology, Universität der Bundeswehr München, Neubiberg, Germany
[d] Department for Anatomy and Cell Biology, Ludwig-Maximilians Universität München, Germany

ARTICLE INFO

Article history:
Received 24 July 2015
Accepted 25 July 2015
Available online xxx

Keywords:
Microbeam
Ion irradiation
Dicentric assay
Mathematical modeling
DSB distribution

ABSTRACT

In conventional experiments on biological effects of radiation types of diverse quality, micrometer-scale double-strand break (DSB) clustering is inherently interlinked with clustering of energy deposition events on nanometer scale relevant for DSB induction. Due to this limitation, the role of the micrometer and nanometer scales in diverse biological endpoints cannot be fully separated. To address this issue, hybrid human-hamster A_L cells have been irradiated with 45 MeV (60 keV/μm) lithium ions or 20 MeV (2.6 keV/μm) protons quasi-homogeneously distributed or focused to 0.5×1 μm^2 spots on regular matrix patterns (point distances up to 10.6×10.6 μm), with pre-defined particle numbers per spot to provide the same mean dose of 1.7 Gy. The yields of dicentrics and their distribution among cells have been scored. In parallel, track-structure based simulations of DSB induction and chromosome aberration formation with PARTRAC have been performed. The results show that the sub-micrometer beam focusing does not enhance DSB yields, but significantly affects the DSB distribution within the nucleus and increases the chance to form DSB pairs in close proximity, which may lead to increased yields of chromosome aberrations. Indeed, the experiments show that focusing 20 lithium ions or 451 protons per spot on a 10.6 μm grid induces two or three times more dicentrics, respectively, than a quasi-homogenous irradiation. The simulations reproduce the data in part, but in part suggest more complex behavior such as saturation or overkill not seen in the experiments. The direct experimental demonstration that sub-micrometer clustering of DSB plays a critical role in the induction of dicentrics improves the knowledge on the mechanisms by which these lethal lesions arise, and indicates how the assumptions of the biophysical model could be improved. It also provides a better understanding of the increased biological effectiveness of high-LET radiation.

© 2015 Elsevier B.V. All rights reserved.

1. Introduction

Chromosomal aberrations are an important endpoint in radiation biology [1]. They link the induction and repair of DNA damage and chromosomes with cell survival [2,3], and are thus relevant for radiation therapy. Chromosome aberrations are also associated with cancer [4].

Dicentric chromosomes are commonly considered as lethal chromosomal aberrations. Elucidating the question how their induction relates to temporal and spatial patterns of chromosome breakage is clearly of relevance for the basic understanding of the mechanisms underlying biological effects of radiation. Another area motivating studies on this issue corresponds to laser-generated particles. These represent a potentially promising option by combining a hopefully compact, cost-effective unit with the well-known physical and biological advantages of proton and ion radiotherapy. Due to the short pulse duration (typically in nanosecond region), laser-generated particles may be temporarily correlated on nanosecond timescales, so that their biological effec-

* Corresponding author. Fax: +49 89 4140 4301.
E-mail address: Schmid@lrz.tu-muenchen.de (T.E. Schmid).
[1] These authors contributed equally to this work.

http://dx.doi.org/10.1016/j.mrgentox.2015.07.015
1383-5718/© 2015 Elsevier B.V. All rights reserved.

Please cite this article in press as: T.E. Schmid, et al., Sub-micrometer 20 MeV protons or 45 MeV lithium spot irradiation enhances yields of dicentric chromosomes due to clustering of DNA double-strand breaks, Mutat. Res.: Genet. Toxicol. Environ. Mutagen. (2015), http://dx.doi.org/10.1016/j.mrgentox.2015.07.015

tiveness could differ from that of particles generated by standard sources.

Regarding the temporal distribution of DNA damage, theoretical studies with the biophysical track-structure based simulation tool PARTRAC have predicted significant effects on DNA double-strand break (DSB) yields from interactions between two tracks only if they were applied in spatial (<10 nm) and temporal (<10 ns) vicinity; this could be the case only if very high particle yields were generated in very short pulses [5]. Using the ion microprobe SNAKE (Superconducting Nanoprobe for Applied nuclear [Kern] physics Experiments) facility of the 14 MV Munich tandem accelerator, no significant difference has been determined in the induction of dicentrics in human-hamster hybrid A_L cells for 20 MeV protons between pulsed (exposure with 1-ns pulse durations) and continuous (applied over 150 ms) irradiation modes [6]. Also no evidence for a different relative biological effectiveness (RBE) was observed between pulsed and continuous 20 MeV protons when the induction of micronuclei was analyzed as an alternative measure to score structural chromosome aberrations in HeLa cells or in keratinocytes of a 3D human reconstructed skin tissue [7,8]. Furthermore, also in vivo no significant difference in tumor growth delay was observed in tumor-bearing mice after irradiation with a single dose of 20 Gy applied in a pulsed or continuous mode [9,10].

Although the biological effectiveness is not influenced by the time course of dose deposition in the studied range, spatial distributions of energy deposition events and the resulting DSB distributions do affect the outcome as shown already in the 70ies and 80ies of the last century using spatially correlated ions produced from diatomic ions [11]. Recently, an enhanced yield of dicentrics was observed in A_L cells by spot application of a bunch of 20 MeV protons (with linear energy transfer, LET, of 2.65 keV/μm) compared to a quasi-homogeneous irradiation [12].

The present investigation aims to elucidate in more detail how the induction of dicentrics depends on the spatial distribution of the dose deposition and DNA damage. Experiments in A_L cells have been performed with 45 MeV lithium ions and 20 MeV protons, using four submicrometer irradiation fields within discrete matrix modes up to 10.6×10.6 μm under matched culture and evaluation conditions. Data obtained earlier under identical conditions for irradiation with 55 MeV carbon ions on a 5.4×5.4 μm grid [12] have been included in the present analysis too.

To improve the mechanistic understanding of the observations and to enable drawing implications on spatial scales relevant for dicentrics induction, the experiments have been complemented with a corresponding PARTRAC modelling study. PARTRAC is a state-of-the-art tool for Monte Carlo simulations of radiation track structures, damage induction in cellular DNA, double-strand break repair [13] and the formation of chromosomal aberrations [14]. The code and the underlying models have been thoroughly tested against physical, chemical and biological data. In particular, PARTRAC has been shown to provide solid predictions of DNA damage from direct (unscavengeable) and indirect (scavengeable, •OH-mediated) effects including DSB yields and DNA fragmentation patterns for low- and high-LET radiations [13,15].

Recent PARTRAC extensions to DSB repair by non-homologous end-joining (NHEJ) and the induction of chromosome aberrations [14,16,17] are still subject to further developments. Simulated yields of dicentrics in human fibroblasts irradiated by γ-rays and α-particles have provided correct dose dependence but systematically overestimated measured data in absolute terms [14]. Nevertheless, in principle the code should be capable of predicting the impact of ion focusing on the formation of dicentrics, providing at least their relative yields for different irradiation patterns. Indeed, PARTRAC calculations of dicentrics for the irradiation patterns used in the pioneering experiments [12] reproduced the 4-fold increased yield of dicentrics after single 55 MeV carbon ions compared to quasi-homogeneous 20 MeV protons, and showed for focused protons an enhanced yield, which however exceeded the experimental result [18].

The present PARTRAC calculations provide another, even more stringent test of its mechanistic approach for interchromosomal misrejoining events. To take into account the key difference in chromosome numbers between the A_L human-hybrid cells used in the experiments (21CHO chromosomes plus human chromosome 11) and the human cell models (46 chromosomes), A_L nuclei have been modelled in PARTRAC by considering the 11 largest human chromosome pairs. Energy deposition events, radical attacks, DNA damage, and its processing by the NHEJ and the resulting chromosome aberrations have been simulated for diverse irradiation patterns. Since the agreement of model calculations with the experimental data is not perfect the basic hypotheses in the chromosomal aberration model in PARTRAC should be revised. Nevertheless, the reported combination of experiments and modelling does provide useful insights regarding spatial scales influential in dicentrics formation. Nevertheless, the reported combination of experiments and modelling does provide useful insights regarding spatial scales influential in dicentrics formation.

2. Materials and methods

2.1. Cell line

In the experiments the A_L cell line was used, established in our laboratory to investigate structural or functional chromosome aberrations after exposure to ionizing or non-ionizing radiation. This cell line was originally derived from the Chinese hamster ovary-K1 (CHO-K1) wild-type cell line, a subclone of an adult Chinese hamster (*Cricetulus griseus*). The A_L cells contain a standard set of CHO-K1 chromosomes plus a single human chromosome 11. Our previous chromosome analysis showed a modal number of 22 chromosomes (85% of analyzed cells); 15% of the analyzed cells had a loss or gain of chromosomes [6]. The cells were grown as monolayer cultures in RPMI-1640 medium (Sigma, Seelze, Germany) supplemented with 16% fetal calf serum and antibiotics (penicillin/streptomycin; Sigma, Seelze, Germany). The cell monolayers were maintained at 37 °C in a humidified atmosphere of 5% CO_2 in air. Under these growth conditions, the A_L cells had a doubling time of 18 h.

2.2. Cell irradiation with 45 MeV lithium ions or 20 MeV protons

For each experiment, a frozen aliquot of A_L cells from the same stock culture was thawed and seeded as cultures with exponentially growing unsynchronized cells into special irradiation containers [8,19]. The irradiations were performed at the ion microprobe SNAKE adopted for use in biological analysis [19,20] which allows the microirradiation of defined cell nuclei with single or counted protons and heavier ions as described in detail previously [21]. In brief, irradiation containers were built by stretching and clamping a 6 μm Mylar foil between two stainless steel plates. About 30,000 A_L cells were placed on this carrier foil which was pretreated with Cell-TAK (BD Bioscience). Shortly before irradiation, about half of the culture medium was removed and the irradiation containers were tightly closed by clamping a second 6 μm Mylar foil. The A_L cell monolayers were irradiated at room temperature of about 22 °C. During irradiation, the container with the cell monolayer, mounted directly behind the beam exit nozzle, was placed vertically in the focal plane of the ion microbeam. In this setup, the cells were not covered by medium, but residual medium in a reservoir ensured a saturated atmosphere.

Please cite this article in press as: T.E. Schmid, et al., Sub-micrometer 20 MeV protons or 45 MeV lithium spot irradiation enhances yields of dicentric chromosomes due to clustering of DNA double-strand breaks, Mutat. Res.: Genet. Toxicol. Environ. Mutagen. (2015), http://dx.doi.org/10.1016/j.mrgentox.2015.07.015

In this irradiation geometry, pre-defined numbers of either 45 MeV lithium ions or 20 MeV protons focused to spots of about 0.5 μm × 1 μm size (full width at half maximum, FWHM), and spots were applied on a regular rectangular matrix with 2.3–10.6 μm grid size as described previously [12]. For a quasi-homogeneous irradiation 4 protons were applied on a grid of 1 × 1 μm. The particles were transported in a vacuum to the beam exit nozzle covered with 7.5 μm kapton foil, traversed 30 μm of air and traversed the 6 μm thick cell carrier foil before hitting the cells, i.e. the total water-equivalent thickness of material traversed before hitting the cells was about 16 μm. Typically, the total time required for sample preparation and irradiation, i.e. the time outside of the CO_2 incubator, was less than 15 min, including about 12 min in the upright position. Under these conditions, there were no differences in the number of chromosome aberrations in non-irradiated cells and cell samples remaining in the incubator [6].

To demonstrate reproducibility as well as inter-test variability, two independent experiments were carried out, mostly with two replicates for exposure of A_L cells to 45 MeV lithium ions or 20 MeV protons. Each irradiation was done not targeted to single cells but in a regular pattern on a central area of 3 mm diameter, using the same average dose of 1.7 Gy; the dose has been calculated from the number of ions per spot, grid size, and LET-energy relation provided by the SRIM code [22]. As listed in Tables 1 and 2, counted ions of both radiation qualities were applied in a focused mode to submicrometer irradiation fields within discrete matrixes of 5.4 × 5.4 μm, 7.6 × 7.6 μm, and 10.6 × 10.6 μm. In addition, a quasi-homogeneous exposure has been carried out applying single lithium ions within a matrix of 2.3 × 2.3 μm or 4 counted protons within a matrix of 1 × 1 μm. As previously noted [12], the use of counted ions allows a very precise dose application with nearly no fluctuations. Since the same experimental setup was used to prepare the submicrometer beam size for irradiation with counted ions in focused and quasi-homogenous mode, potential systematic errors were compensated by direct comparison of the results from the different irradiation modes. The systematic dose uncertainty is only given by the uncertainty of the LET of the particles and the calibrations of the scanning unit, which have been estimated to be less than 3% [12].

2.3. Post-irradiation culture and chromosome analysis

The cell culture conditions have been described in detail previously [12]. In brief, immediately after irradiation, a 1 mm^2 biopsy punch of A_L cells from the central part of the irradiated area was cut out. The cells were trypsinized and reseeded in 4 ml RPMI-1640 medium supplemented with 20% fetal calf serum and antibiotics (penicillin/streptomycin) and incubated at 37 °C in a humidified atmosphere of 5% CO_2 in air. Colcemid (Life Technologies Darmstadt, Germany) at the concentration of 0.1 μg/ml was present in the cultures during the last 4 h of the total incubation time of 20 h. Chromosome preparation and Giemsa staining were carried out according to our standardized laboratory procedure originally described for human lymphocytes [23]. All object slides were coded. Only complete cells containing the modal number of 22 chromosomes were analyzed for dicentrics. Tricentric chromosomes were counted as two dicentrics, and similarly chromosomes with N > 3 centromeres, if present, as N-1 dicentrics. Since the measured dicentric yields are generally used as the most characteristic and quantitatively reproducible biological endpoint of radiation-induced chromosome-type aberrations, only the data for dicentrics were used in the quantitative analysis, although the yields of centric rings and acentric fragments were also determined.

2.4. Statistical analysis of the data

A null hypothesis that the observed differences between the mean frequencies of dicentrics (±SE) determined either in two replicates of an experiment or in two independently performed experiments are not different was tested according to the *z*-test statistics. Since the conditions for the application of the normal probability distribution hold for these data (i.e. both sample sizes are much larger than 100 cells and the products of sample sizes and proportions are greater than five), this statistical procedure could be applied. A difference at the two-sided *p*-value <0.05 was considered statistically significant.

The intercellular distribution of aberrations has been tested for deviating from a Poisson distribution. To this point, a test quantity *u* has been used which is related to the numbers of cells analyzed (N) and dicentrics scored (*n*), the dispersion ratio (variance σ^2 over mean *y* = n/N) by Schmid et al. [24]

$$u = \left(\frac{\sigma^2}{y} - 1\right)\sqrt{\frac{N-1}{2(1-\frac{1}{n})}}$$

For a Poisson distribution, σ^2 = y and hence *u* = 0. Values of *u* in excess of 1.96 indicate overdispersion at the 5% level of significance.

2.5. Model calculations

The model for chromosome aberration induction within the PARTRAC suite of biophysical codes combines the simulation of radiation tracks, chromatin structures, initial DNA damage, kinetics of DSB repair and DNA end mobility.

2.5.1. Modelling DNA damage

Radiation tracks are simulated on an event-by-event basis, i.e. all relevant interactions of the primary ion as well as of all secondary electrons are followed. Subsequently, the energy deposition events taking place in the volume of DNA are scored as direct effects. Events outside but close to DNA are passed to the pre-chemical and chemical modules in which the formation, diffusion and mutual reactions of reactive species are modelled. Attacks of •OH radicals on the DNA are scored as indirect effects. These reactive species have a diffusion range of about 5 nm in the nuclear environment. The DNA and chromatin target structures accounted for in PARTRAC include atomic models of base pairs, nucleosome, chromatin fibre, chromatin loops and domains, and chromosome territories within spherical or ellipsoidal human cell nuclei. The directly and indirectly induced DNA damage is analyzed with respect to damage types including lesion complexity.

The cell nucleus model for A_L cells used in this work has been generated from the 22 largest chromosomes with 4.2×10^9 base pairs (bp) of the standard PARTRAC model for a human lymphocyte which has a spherical nucleus with 10 μm diameter [13]. Preliminary calculations have indicated that such a spherical model nucleus irradiated from random directions provides a better modelling basis than a unique distribution of chromosomes in an ellipsoidal nucleus irradiated in parallel to the short axis. It would be preferable to consider an ensemble of ellipsoidal nuclei with varying chromosomal arrangements, but this could not be achieved within the present study. No differentiation between heterochromatic and euchromatic regions was considered.

2.5.2. Modelling DSB repair and induction of chromosome aberrations

The calculated DNA damage is used as an input for modelling the non-homologous end-joining (NHEJ) repair pathway for DSB. The simulation starts with a DSB recognition and chromatin remodelling step after which the DSB is assumed to open, i.e. form

Please cite this article in press as: T.E. Schmid, et al., Sub-micrometer 20 MeV protons or 45 MeV lithium spot irradiation enhances yields of dicentric chromosomes due to clustering of DNA double-strand breaks, Mutat. Res.: Genet. Toxicol. Environ. Mutagen. (2015), http://dx.doi.org/10.1016/j.mrgentox.2015.07.015

Table 1
Frequencies (±standard errors of the mean, SE) of dicentrics and their intercellular distributions in A_L cells following exposure to 1.7 Gy of 45 MeV lithium ions.

Matrix exposure (μm)	Counted ions	Cells scored	Dicentrics per cell (±SE)	Intercellular distribution of dicentrics						
				0	1	2	3	4	σ^2/y	*u*-Value
Control*	–	5312[§]	0.0006 ± 0.0003	5309	3				1.0	−0.02
Control	–	2000	0.0010 ± 0.0006	1998	2				1.0	−0.01
	Experiment I									
10.6 × 10.6	20	238	0.206 ± 0.034	200	29	7	2		1.33	3.63
10.6 × 10.6	20	203	0.187 ± 0.032	171	26	6			1.13	1.36
7.6 × 7.6	10	272	0.151 ± 0.026	238	28	5	1		1.24	2.88
7.6 × 7.6	10	208	0.134 ± 0.028	185	18	5			1.23	2.43
5.4 × 5.4	5	281	0.121 ± 0.025	254	22	4	0	1	1.47	5.67
5.4 × 5.4	5	242	0.120 ± 0.025	218	19	5			1.23	2.57
2.3 × 2.3	1	241	0.108 ± 0.023	219	18	4			1.21	2.29
2.3 × 2.3	1	227	0.093 ± 0.022	209	15	3			1.20	2.16
	Experiment II									
10.6 × 10.6	20	236	0.186 ± 0.028	196	36	4			1.00	−0.02
10.6 × 10.6	20	220	0.218 ± 0.032	176	41	2	1		0.99	−0.60
7.6 × 7.6	10	212	0.142 ± 0.028	187	20	5			1.20	2.06
7.6 × 7.6	10	223	0.153 ± 0.029	194	25	3	1		1.21	2.20
5.4 × 5.4	5	162	0.111 ± 0.028	146	14	2			1.09	1.89
5.4 × 5.4	5	219	0.123 ± 0.027	197	18	3	1		1.33	3.48
2.3 × 2.3	1	232	0.095 ± 0.023	214	14	4			1.27	3.02
2.3 × 2.3	1	241	0.091 ± 0.021	222	16	3			1.19	2.09

[§] Control, background frequency [12]; σ^2/y, dispersion ratio; *u*-value, test quantity.

Table 2
Frequency (±SE) of dicentrics and their intercellular distribution in A_L cells following exposure to 1.7 Gy of 20 MeV protons within different matrix exposures; σ^2/y, dispersion ratio; *u*-value, test quantity.

Matrix exposure (μm)	Counted ions	Cells scored	Dicentrics per cell (±SE)	Intercellular distribution of dicentrics					
				0	1	2	3	σ^2/y	*u*-Value
	Experiment I								
10.6 × 10.6	451	168	0.131 ± 0.029	148	18	2		1.06	0.54
10.6 × 10.6	451	126	0.143 ± 0.039	111	13	1	1	1.31	2.54
7.6 × 7.6	232	210	0.105 ± 0.024	191	16	3		1.17	1.82
7.6 × 7.6	232	144	0.125 ± 0.031	128	14	2		1.11	0.92
5.4 × 5.4	117	232	0.082 ± 0.020	215	15	2		1.13	1.47
5.4 × 5.4	117	245	0.069 ± 0.017	229	15	1		1.04	0.55
hom[a]	1	212	0.047 ± 0.016	203	8	1		1.16	1.71
hom[a]	1	266	0.049 ± 0.014	254	11	1		1.11	1.31
	Experiment II								
10.6 × 10.6	451	218	0.138 ± 0.028	192	23	2	1	1.20	2.13
7.6 × 7.6	232	171	0.117 ± 0.030	155	12	4		1.29	2.75
5.4 × 5.4	117	262	0.096 ± 0.021	240	19	3		1.15	1.74
hom[a]	1	210	0.043 ± 0.014	201	9			0.96	−0.42

[a] Quasi-homogeneous irradiation corresponding to 1 proton per 0.5 × 0.5 μm matrix point.

two mobile DNA ends (chromatin broken ends). The two ends are allowed to diffuse around limited by the genomic distance to the nearest nuclear attachment site assuming a moderately condensed fiber with 30 nm/kbp; each chromosome is organized in loops between such nuclear attachment sites separated by up to about 100 kbp. By this, semi-confined diffusion mobility is considered in the model; it results in a mean distance of 0.55 μm between still unrejoined DNA ends and their nuclear attachment sites after 1 day repair time.

In parallel with diffusive mobility of the DNA ends, the temporal dimension of the repair process is considered as shown in Fig. 1, reflecting the attachment and action of repair enzymes. After chromatin remodelling (step 1), Ku70/80 heterodimer has to bind to an end (step 4), followed by the DNA-PKcs subunit (step 6), forming together the functional DNA-PK enzyme. When two ends with DNA-PK attached happen to be in close vicinity (<25 nm distance), they form a synaptic complex (step 8). The two DNA-PK molecules cross-phosphorylate each other, and further repair proteins bind and perform their tasks (step 9). In particular, end processing and removal of additional strand breaks and/or base lesions take place (step 10) before the final ligation of the two DNA ends happens (step 11). Occasional enzyme detachment and processing failures are considered too (steps 7, 12, 13).

Note that in agreement with the real case, not only the original partners, i.e. the two broken DNA ends of one DSB, but also another pair of DNA ends may get ligated. This occurs when a free end diffusing around with attached DNA-PK finds an incorrect partner ready for joining, e.g. because its original partner, though perhaps in proximity, lacks DNA-PK and thus cannot be ligated yet. Whenever such incorrect joining takes place, information is stored on the chromosomal origin of the joined fragments and whether centromere regions are involved. Further details on the methods and specific assumptions used can be found elsewhere [13,14].

Model parameters as described by Friedland et al. [14] were used for the simulation of DNA damage, DSB repair and the induction of chromosomal aberrations, with two exceptions regarding the repair model: the period for which the formation of chromosomal aberrations was traced has been reduced from 4 days to 1 day to reflect the experimental protocol, and the cleaning of dirty DNA ends (step 12) has been further retarded to yield an expected higher fraction of the slowly rejoining DSB in the repair kinetic after C ion irradiation.

Please cite this article in press as: T.E. Schmid, et al., Sub-micrometer 20 MeV protons or 45 MeV lithium spot irradiation enhances yields of dicentric chromosomes due to clustering of DNA double-strand breaks, Mutat. Res.: Genet. Toxicol. Environ. Mutagen. (2015), http://dx.doi.org/10.1016/j.mrgentox.2015.07.015

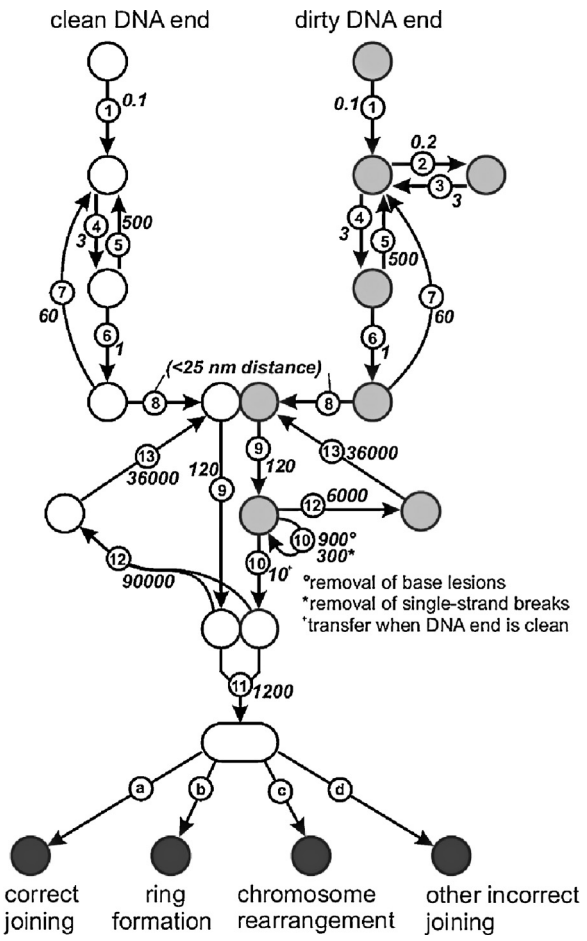

Fig. 1. Scheme of DSB repair and chromosomal aberration formation model. Numbers in circles refer to individual steps in first order kinetics (see text), numbers in italics are corresponding time constants in seconds.

The following hypotheses have been incorporated in the present DSB repair model: broken DNA ends rejoin correctly after attachment of Ku70/80 and DNA-PKcs provided that they are still in spatial vicinity. For dirty DNA ends (i.e., DNA ends carrying further single-strand breaks or base damage), the attachment of Ku and DNA-PKcs is frequently delayed (steps 2 and 3), therefore, loss of spatial vicinity occurs with higher probability compared to clean DNA ends. Very short DNA fragments (<25 bp) are unable to be ligated as they cannot attach the repair enzymes. Since no break-up of synaptic complexes is included in the scheme, the formation of synaptic complexes which corresponds to a rather early phase of DSB repair decides on the repair outcome. The outcome is classified into four principle categories: correct rejoining, formation of rings, intrachromosomal misrejoining and interchromosomal misrejoining; these are complemented by the two classes of unrejoinable and as yet unrejoined DSB ends. A dicentric chromosome has been assumed cytogenetically detectable only if the two centromeric regions were present completely and embedded in a DNA fragment of at least 15 Mbp size.

2.5.3. Modelling focused irradiation on matrix grid

The layout of a radiation source corresponding to the experimental setup has been defined in the track structure module of PARTRAC. Given numbers of primary ions with given energy have been started in bunches with two-dimensional Gaussian distribution of elliptical shape (0.5 μm × 1 μm FWHM) around centres on a quadratic matrix of a given size. The source matrix has been located in a layer at 20 μm distance from the centre of the nucleus, reflecting the water-equivalent thickness of material traversed by the particles before reaching the cells (and 10 μm diameter of the model cell nucleus). All ions were started exactly perpendicular to the source layer. The source matrix has consisted of 30 × 30 spots for 0.5 μm grid (single protons per spot), 5 × 5 spots for 2.3 μm grid (single Li ions), 3 × 3 spots for 5.4 μm and 7.6 μm grids, and 2 × 2 spots for 10.6 μm grid (p, Li and C ions), respectively. This setup has ensured sufficient coverage of cell nuclei by the matrix while avoiding unnecessary long computation times.

For each irradiation setup 200 runs were calculated, i.e. irradiation of 200 cells located randomly with respect to the irradiation matrix pattern has been simulated. This random localization and orientation has been realized by shifting the source matrix between succeeding runs by random displacement up to half the grid size in both axes normal to the emission direction and by rotating the matrix randomly in three dimensions around the centre of the nucleus.

3. Results

3.1. Dicentric data for cell exposure to 45 MeV lithium ions or 20 MeV protons

The detailed results for dicentrics and their intercellular distribution in A_L cells are presented in Tables 1 and 2 together with the corresponding background frequencies. The spontaneous frequency of 0.0010 ± 0.0006 determined in 2000 cells (Table 1) of the present experiments is not statistically different from the value of 0.0006 ± 0.0003 obtained in 5312 cells ($z = 0.60$, $p = 0.55$) previously reported [12]. In a total of 6121 analyzed cells irradiated with 1.7 Gy of 45 MeV lithium ions or 20 MeV protons, 734 dicentrics (including 12 tricentrics) were observed at the four spatial irradiation modes. Whereas 10 tricentrics were observed in a total of 3657 cells exposed to lithium ions, practically independently of the spatial irradiation mode, only 2 tricentrics could be found in 2464 cells exposed to protons, only in the 10.6 × 10.6 μm matrix. At 12 from 16 exposures to 20 lithium ions and at 3 from 12 exposures to 117 protons per spot, the intercellular distribution of dicentrics was over-dispersed (p-values from 2.06 to 5.67), as assessed by the test quantity u [24]. The dicentric data determined for exposure of A_L cells to 45 MeV lithium ions are summarized in Table 1. No significant differences have been determined between the yields of dicentrics which were observed in any exposure mode between experiment I (p-values from 0.64 to 0.98) and experiment II (p-values from 0.45 to 0.90). The corresponding dicentric data obtained for exposure to 20 MeV protons are shown in Table 2, applying the same four submicrometer irradiation fields. In accordance with the results for exposure to lithium ions, there are no significant differences between the dicentric yields determined in the two replicates of experiment I (p-values from 0.61 and 0.93). Therefore, the yields of dicentrics from the replicates within the different experiments were pooled; the resulting mean values of dicentrics in experiments I and II are plotted in Fig. 2. The panels show a similar increase of dicentrics yields induced by both radiation qualities between the four irradiation modes. Further, since no significant differences could have been determined between the pooled dicentric yields of experiments I and II induced either by 45 MeV lithium ions (p-values from 0.76 to 0.92) or by 20 MeV protons (p-values from 0.42 to 0.96), also the results of experiments I and II could have been pooled. The pooled dicentric data and their intercellular distributions in experiments I and II are given at the diverse exposure modes in Table 3. Increasing focusing gradually increases the yields of dicentrics for both protons and lithium ions. The highest degree of focusing analyzed here, namely 451 pro-

Please cite this article in press as: T.E. Schmid, et al., Sub-micrometer 20 MeV protons or 45 MeV lithium spot irradiation enhances yields of dicentric chromosomes due to clustering of DNA double-strand breaks, Mutat. Res.: Genet. Toxicol. Environ. Mutagen. (2015), http://dx.doi.org/10.1016/j.mrgentox.2015.07.015

Table 3
RBE (±SE) of 45 MeV lithium ions or 20 MeV protons relative to 70 kV X-rays derived for the induction of dicentrics in A_L cells at different matrix conditions. Dicentric data and their intercellular distribution (σ^2/y and *u*-value) are given as mean values from two independently performed experiments at an average dose of 1.7 Gy.

Particle	Matrix exposure (μm)	Counted ions	Cells scored	Dicentrics per cell (±SE)	σ^2/y	*u*-Value	X-ray dose	RBE (±SE)
Li	10.6 × 10.6	20	897	0.200 ± 0.016	1.11	2.43	5.51	3.24 ± 0.29
Li	7.6 × 7.6	10	915	0.145 ± 0.014	1.22	4.65	4.57	2.69 ± 0.24
Li	5.4 × 5.4	5	904	0.120 ± 0.013	1.31	6.57	4.08	2.40 ± 0.22
Li	2.3 × 2.3	1	941	0.097 ± 0.011	1.21	4.63	3.59	2.11 ± 0.20
P	10.6 × 10.6	451	512	0.137 ± 0.018	1.18	2.90	4.42	2.60 ± 0.27
p	7.6 × 7.6	232	525	0.114 ± 0.016	1.19	3.07	3.96	2.33 ± 0.25
p	5.4 × 5.4	117	739	0.083 ± 0.011	1.12	2.24	3.26	1.92 ± 0.20
p	hom[a]	1	688	0.047 ± 0.009	1.08	1.51	2.27	1.33 ± 0.19
C[§]	5.4 × 5.4	1	1694	0.197 ± 0.012	1.26	7.59	5.47	3.21 ± 0.27

[a] Quasi-homogeneous irradiation corresponding to 1 proton per 0.5 × 0.5 μm matrix point.
[§] For comparison, previous data are given for exposure of A_L cells to 1.7 Gy of 55 MeV ^{12}C ions [12]; σ^2/ y, dispersion ratio; *u*-value, test quantity.

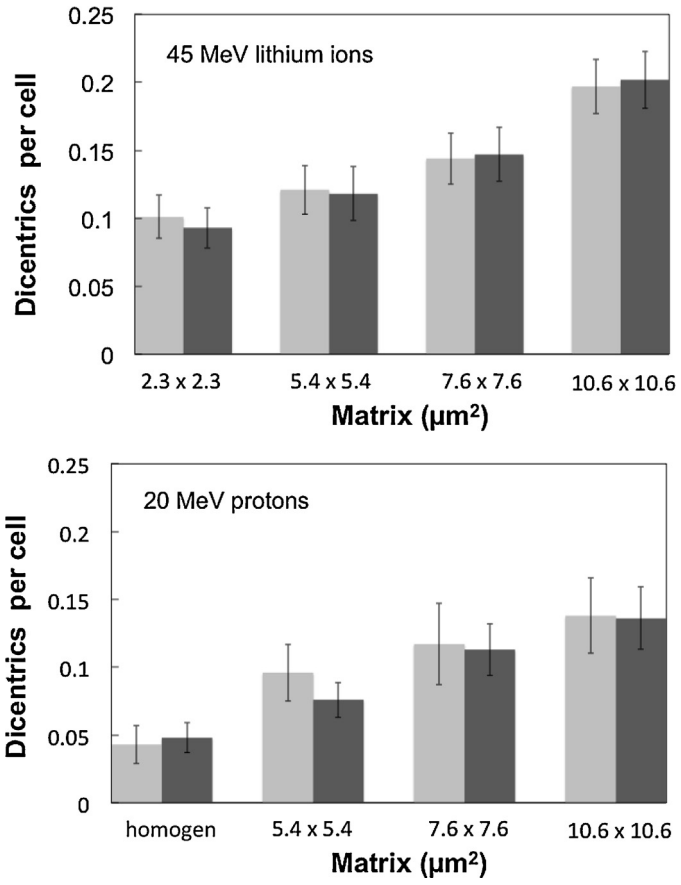

Fig. 2. Measured frequency of dicentrics induced by 1.7 Gy of 45 MeV lithium ions (upper panel) or 20 MeV protons (lower panel) in AL cells using different matrix conditions. Each of the values is the pooled result of two independently performed experiments I (light columns) and experiments II (dark columns). Standard errors of the mean (SE) are indicated by vertical bars.

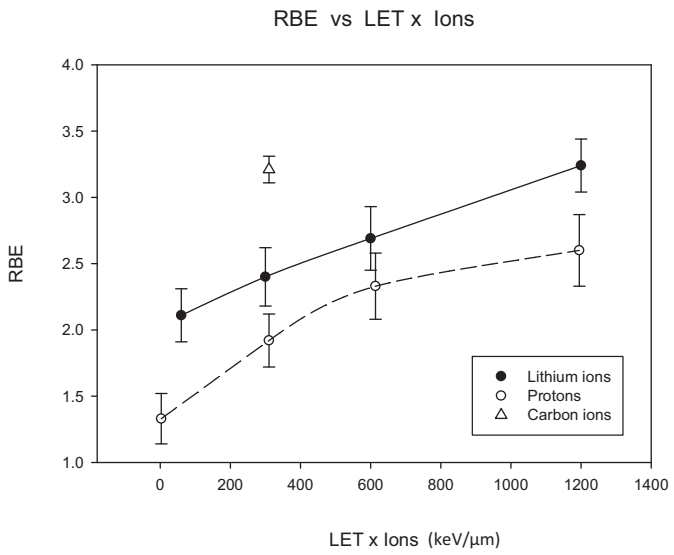

Fig. 3. Measured RBE (±SE) of 45 MeV lithium ions and 20 MeV protons with respect to 70 kV X-rays. The values are evaluated against the product of LET and number of ions per matrix point using the four submicrometer irradiation fields at the same average dose of 1.7 Gy. The previously reported RBE for 55 MeV 12 C irradiation on a 5.4 × 5.4 μm matrix is included [12].

tons or 20 lithium ions per spot on the 10.6 μm grid, increases the induction of dicentrics three- or two-fold, respectively.

3.2. RBE dependence of 45 MeV lithium ions and 20 MeV protons on spatial irradiation modes

Conventional differences in radiobiological effects are also expressed in terms of RBE. In order to calculate the influence of the four spatial irradiation modes on the RBE of both radiation qualities, our previously established dose-response curve of dicentrics in A_L cells exposed to 70 kV X-rays [12] was used. For this reference radiation quality, a weighted least-squares approximation was applied to fit the dicentric data with the linear-quadratic function, $y = c + \alpha D + \beta D^2$, where y is the dicentric yield, D is the radiation dose, c is the background frequency of dicentrics, and α and β are coefficients. The resulting linear-quadratic coefficients (±SE) are $c = 0.0006 \pm 0.0005$, $\alpha = 0.010 \pm 0.003\ \mathrm{Gy}^{-1}$ and $\beta = 0.0048 \pm 0.0012\ \mathrm{Gy}^{-2}$. The RBE values were calculated using the X-ray doses that produced the same response as 1.7 Gy of the presently applied radiation qualities, i.e. the necessary X-ray doses have been determined by inverting the fitted dose–response curve. As the fit parameters are highly correlated for calculation of RBE errors, not only the diagonal elements of the covariance matrix, the parameter errors, are taken into account but also the non-diagonal elements, describing the correlation of parameters. A detailed description of the RBE calculation was given previously [12]. The resulting RBE values of 45 MeV lithium ions and 20 MeV protons are given in Table 3. As demonstrated in Fig. 3, the RBE values evaluated against the product of LET and number of ions per matrix point increase with increasing matrix grid size, for both radiation types. In detail, the RBE is significantly higher ($z = 3.21$, $p < 0.001$) when 20 lithium ions were focused per submicrometer spot on a 10.6 × 10.6 μm matrix (RBE = 3.24 ± 0.29) compared to a quasi-homogeneous exposure by single lithium ions on a 2.3 × 2.3 μm matrix (RBE = 2.11 ± 0.20). Comparable findings are obtained for exposure to 20 MeV protons. The RBE is significantly higher ($z = 3.85$, $p < 0.001$) when 451 protons were focused per spot on a 10.6 × 10.6 μm matrix (RBE = 2.60 ± 0.27) compared to single

Please cite this article in press as: T.E. Schmid, et al., Sub-micrometer 20 MeV protons or 45 MeV lithium spot irradiation enhances yields of dicentric chromosomes due to clustering of DNA double-strand breaks, Mutat. Res.: Genet. Toxicol. Environ. Mutagen. (2015), http://dx.doi.org/10.1016/j.mrgentox.2015.07.015

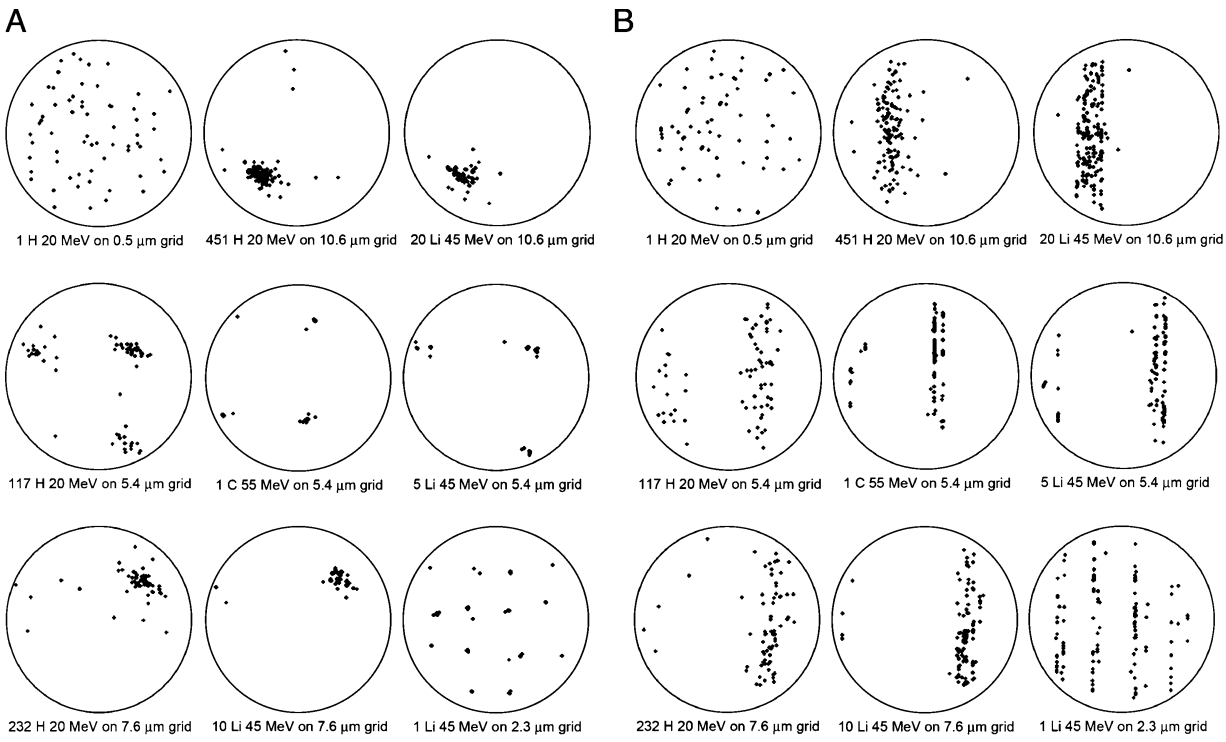

Fig. 4. Calculated distribution of DNA double-strand breaks for all irradiation set-ups. Each point denotes a DSB, circles outline the nucleus.Panel A: projection in beam direction (*z*-axis) on *x*-*y* plane. Panel B: projection perpendicular to beam direction on *x*-*z* plane.

protons on a 0.5×0.5 μm matrix (RBE = 1.33 ± 0.19). Due to the different LET values of both radiation qualities, exposure of A_L cells to single lithium ions on a 2.3×2.3 μm matrix induces a significantly higher RBE of 2.11 ± 0.20 than the RBE of 1.33 ± 0.19 applying single protons on a 0.5×0.5 μm matrix ($z = 2.83$, $p = 0.005$).

3.3. Initial DNA damage

The main results of simulating the initial DNA damage with PARTRAC are listed in Table 4. Single Li ions on a 2.3 μm grid have a 10% higher fluence than the Li ion bunches on larger grids. This leads to significantly higher DSB yields, but otherwise ion focusing has no impact on total amount of initial DNA damage. This holds for DSB yields as well as for the formation of short DNA fragments (<25 bp) that are assumed to be intrinsically unrejoinable in our repair model. The fractions of dirty DNA ends (i.e. DNA ends with nearby single strand breaks or base lesions) are not affected by the focusing, either. All these characteristics of the initial DNA damage reflect the intrinsic properties of individual particle tracks, and (for the three cases studied here) increase with increasing LET. This is particularly pronounced for the numbers of unrejoinable DSB from ultrashort fragments.

The spatial distribution of DSB inside the nucleus reflects both the focusing effect as well as characteristics of the incident particles (Fig. 4). For a quasi-homogeneous proton irradiation (single protons on 0.5 μm grid), the DSB distribution is almost homogeneous (but random). With increasing focusing and/or ions' LET, streaks of DSB can be seen. After C ion irradiation DSB are found along or in close vicinity to the ion trajectories (note that two tracks almost overlap in the *x*-*z* projection, Fig. 4B), whereas for protons a fraction of about 20% of DSB is located outside the spots due to the larger range of δ-electrons which depends on the energy per nucleon of the incident ions (up to 10 μm for 20 MeV protons compared to about 1 μm for carbon ions with 4.5 MeV/nucleon). To further analyze quantitatively the spatial distribution of DSB, histograms of distances are shown in Fig. 5 for DSB pairs on different chromosomes due to protons (Panel A) and lithium or carbon ions (Panel B), compared to pairs of DSB within the same chromosomes (Panel C for protons and Panel D for lithium or carbon ion irradiations). It should be noted that the distributions for inter-chromosomal distances are affected by the morphology of the cell model which e.g. excludes a peak corresponding to the largest grid size in the distributions on Panel A and B. For each chromatin free end (two DNA termini per each DSB), the geometric distances to all other chromatin free ends (in the same nucleus, i.e. same simulation run) have been determined and tallied into histograms for inter- or intra-chromosomal pairs with 100 nm binning. Excluded from this analysis have been ends of DNA fragments which are not linked to nuclear attachment sites (rather short fragments arising from at least two DSB on the same ~100 kbp chromatin loop). For intra-chromosomal pairs of DNA ends (Panels C and D), the frequency in the smallest distance interval is enhanced for all distributions and largely independent of the number of particles per spot. For irradiations with multiple ions per spot a maximum occurs at about 0.7 μm distances likely given by the spot size; the height of this peak is given by the number of particles per spot. For pairs of DNA termini on different chromosomes (Panels A and B), the distance distributions are characterized for irradiations with multiple particles per spot by elevated frequencies for distances between about 1 and 3 μm, again given by the number of ions per spot, and by a peak for grid sizes of 5.4 and 7.6 μm at about this value. A corresponding histogram has also been obtained for single C ions. For single protons a Gaussian distribution around 5 μm is seen corresponding to an almost random distribution of DNA ends within the nucleus; a complex distribution results for single Li ions on 2.3 μm grid.

3.4. Modelling of DSB repair

The simulated repair kinetics (Fig. 6) for the diverse irradiation schemes group mainly according to the ion type: with increasing LET of the incident ions, increased fractions of slowly rejoining DSB are observed. Nevertheless, the characteristic times for repair

Please cite this article in press as: T.E. Schmid, et al., Sub-micrometer 20 MeV protons or 45 MeV lithium spot irradiation enhances yields of dicentric chromosomes due to clustering of DNA double-strand breaks, Mutat. Res.: Genet. Toxicol. Environ. Mutagen. (2015), http://dx.doi.org/10.1016/j.mrgentox.2015.07.015

Table 4
Setup of model calculations and the predicted initial DNA damage.

Particle	Energy (MeV)	Matrix grid (μm)	Number of ions	DSB yield per cell	Fraction of dirty DNA ends (%)	Unrejoinable DNA ends per cell
Li	45	10.6 × 10.6	20	76.0	59.5	5.5
Li	45	7.6 × 7.6	10	75.8	59.0	4.8
Li	45	5.4 × 5.4	5	76.6	59.5	5.4
Li	45	2.3 × 2.3	1	86.8	59.5	5.9
p	20	10.6 × 10.6	451	45.6	36.0	0.8
p	20	7.6 × 7.6	232	46.2	36.0	0.7
p	20	5.4 × 5.4	117	45.5	35.9	1.1
p	20	hom[a]	1	44.1	36.0	0.9
C	55	5.4 × 5.4	1	142	85.7	67

[a] Quasi-homogeneous irradiation corresponding to 1 proton per 0.5 × 0.5 μm matrix point.

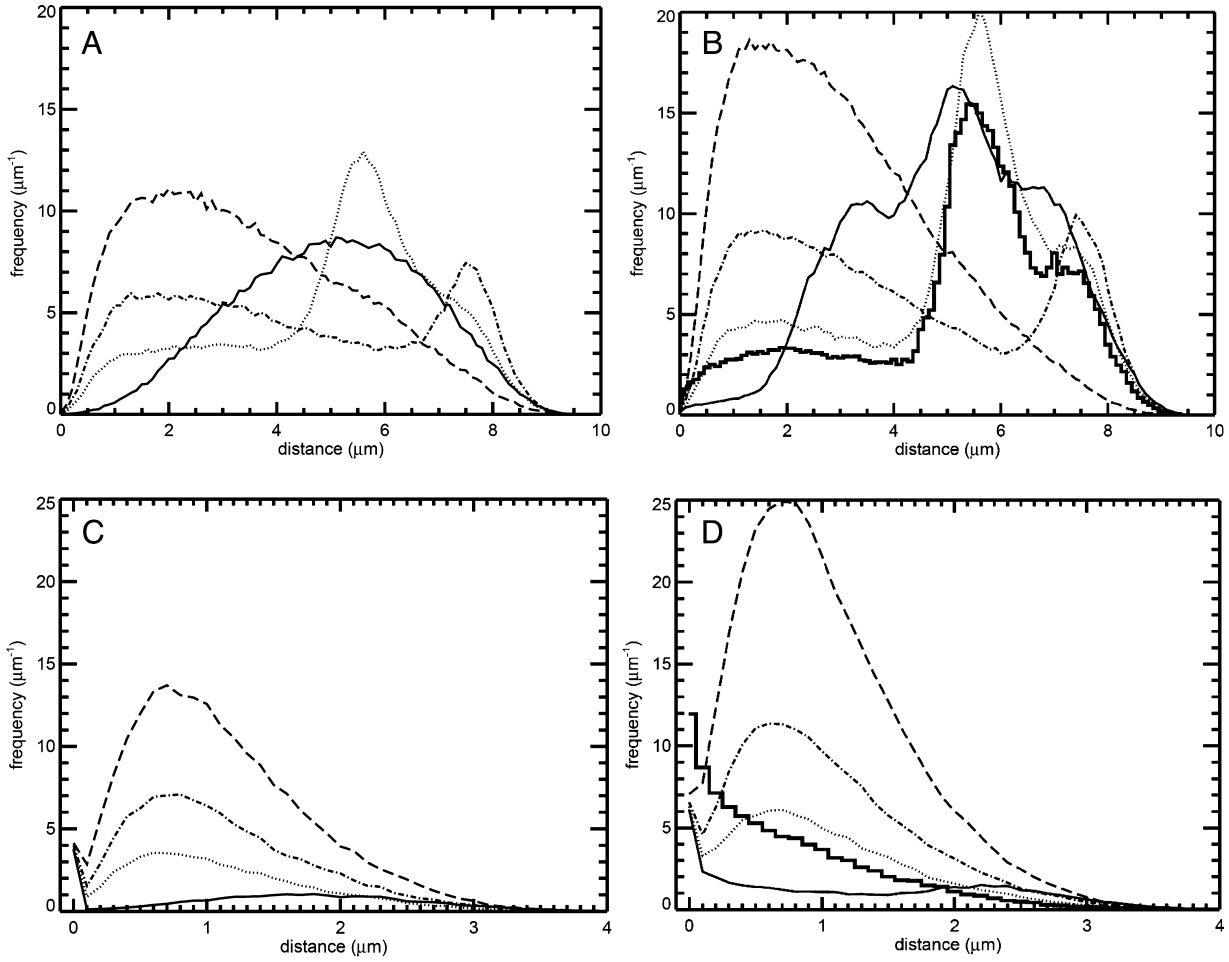

Fig. 5. Calculated distribution of distances between ends of DNA fragments connected to the nuclear matrix. Panel A: DNA ends on different chromosomes after proton irradiation, panel B: DNA ends on different chromosomes after Li or C ion irradiation, panel C: DNA ends on the same chromosome after proton irradiation, panel D: DNA ends on the same chromosomes after Li or C ion irradiation. Thick histogram line: C ions 5.4 μm grid (panels B,D); solid line: protons 0.5 μm grid (A,C) and Li ions 2.3 μm grid (B,D); dotted line: protons (A,C) and Li ions (B,D) 5.4 μm grid; dash-dot line: protons (A,C) and Li ions (B,D) 7.6 μm grid; dashed: protons (A,C) and Li ions (B,D) 10.6 μm grid.

(slopes of the lines) are similar for different particles. Increased numbers of Li ions per spot lead to slightly faster repair. For protons this holds only during the initial phase, but after 10 h more DSB have rejoined after being quasi-homogeneously distributed than for focused protons.

The fraction of unrejoined DNA ends depends only slightly on the grid size or the number of ions per grid point, while the fractions of intra-chromosomally and inter-chromosomally misrejoined DNA ends increase about linearly with the grid size (Fig. 7). Again, these fractions are higher for the ion types with higher LET. The fraction of rings (not shown) increases with the grid size for protons from 0.01 to 0.05 and has a grid size independent fraction of 0.09 for Li ions. On the other hand, the fractions of correctly rejoined DNA ends (not shown) decrease about linearly with the grid size, from 0.89 to 0.52 for protons, from 0.49 to 0.26 for Li ions, and contribute 0.09 for C ions.

3.5. Modelling of dicentrics

For the nine irradiation setups the calculated yields of dicentrics are presented in Fig. 8 together with the experimental results in Table 3. The calculated yields of dicentrics overestimate for quasi-homogeneous protons as well as for single carbon ions the observed yields of dicentrics by about 50%. The model clearly overestimates,

Please cite this article in press as: T.E. Schmid, et al., Sub-micrometer 20 MeV protons or 45 MeV lithium spot irradiation enhances yields of dicentric chromosomes due to clustering of DNA double-strand breaks, Mutat. Res.: Genet. Toxicol. Environ. Mutagen. (2015), http://dx.doi.org/10.1016/j.mrgentox.2015.07.015

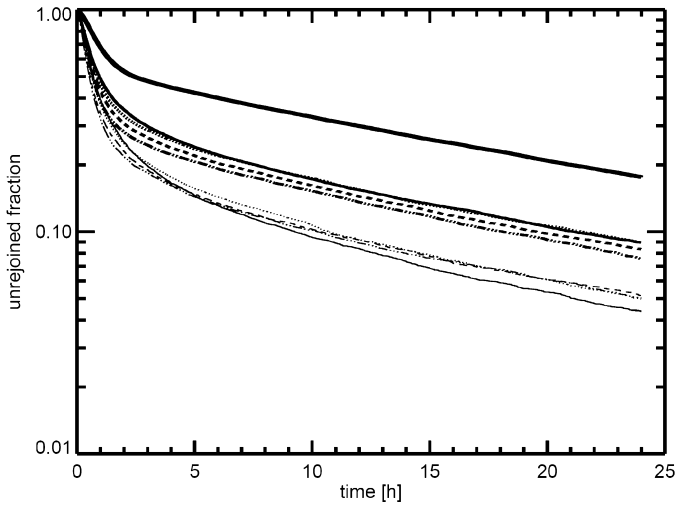

Fig. 6. Calculated DSB rejoining kinetics. Thick line: 55 MeV C ions (5.4 μm grid); medium line: 45 MeV Li ions (solid, dotted, dashed, dash-dot–dot line: 2.3 μm, 5.4 μm, 7.6 μm, 10.6 μm grid, resp.); thin line: 20 MeV protons (solid, dotted, dashed, dash-dot–dot line: 0.5 μm, 5.4 μm, 7.6 μm, 10.6nμm grid, resp.).

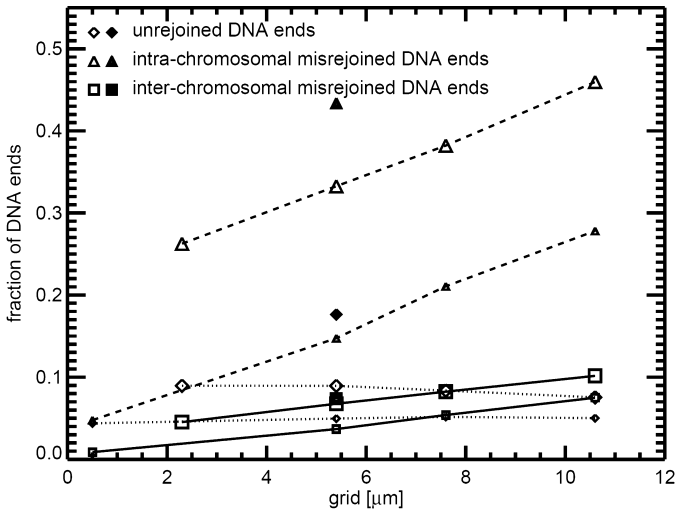

Fig. 7. Calculated fractions of DNA end states after 24 h repair time. Small symbols: 20 MeV proton irradiation; large open symbols: 45 MeV Li ion irradiation; filled symbols: 55 MeV C ion irradiation. Lines are drawn to guide the eyes only (solid: inter-chromosomal misrejoined DNA ends, dashed: intra-chromosomal misrejoined DNA ends, dotted: still unrejoined DNA ends).

more than three-fold, the effects of focusing for protons on the 5.4 and 7.6 μm grids. Li ions on the 2.3 μm and 5.4 μm grids are overestimated about five-fold, and then unlike the experiments, show a decreasing trend with increasing grid sizes. Indications for such a decreasing trend, or at least saturation at grid sizes above 5 μm, can be seen in model predictions for protons as well.

Also shown in Fig. 8 is the calculated total induction of exchange aberrations. These simulation results reproduce quite correctly the measured trends for dicentrics for Li ions and for multiple protons per spot, as well as the relation between the effects of Li and C ions, but overestimate the focusing effect for protons and the relation between the effects of Li ions and protons.

4. Discussion

Conventional radiobiological experiments with different LET radiation types are inherently limited by linkage of radiation track-structure properties on different scales. Namely, with increasing

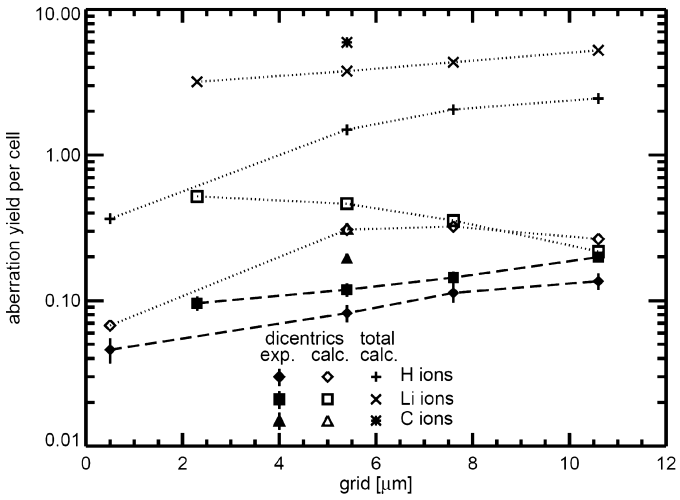

Fig. 8. Simulated yieldsof dicentrics in dependence on the degree of focusing (empty symbols; protons ◊, Li ions □, C ions Δ) compared to the experimental data from Table 3 (filled symbols; protons ♦, Li ions ■, C ions ▲). Also shown are the simulated yields of total chromosomal exchange aberrations (other symbols; protons +, Li ions ×, C ions *). Lines showing the trends in data or simulation results for focused proton and lithium irradiations are drawn to guide the eyes only.

LET, the clustering of energy deposition events and hence also the DNA damage increases both on the nanometer scale relevant for DSB induction and on the (sub-) micrometer scale that governs the spatial distribution of DSB and DNA fragmentation pattern. Conventional experiments can hardly elucidate how these two scales contribute to the increased biological effectiveness of high-LET radiation in terms of induction of chromosomal aberrations or cell killing. The reported microbeam experiments with sub-micrometer focusing of protons or lithium ions represent a novel approach tailored to solve this issue. Indeed, PARTRAC track structure-based simulations, thoroughly benchmarked against data on DSB yields and DNA fragmentation [13,15], show that the nanometer clustering, i.e. yield of DSB, remains constant for a given particle type, independent of the focusing (Table 4). With increasing number of particles per spot (and increasing grid size so that the average dose is kept constant), however, the (sub-) micrometer clustering of DSB increases. The distributions of distances between chromosome free ends (Fig. 5) show the increase in the number of nearby DNA ends from the same as well as from different chromosomes. Consequently, both intra- and inter-chromosomal misrejoining increase with increasing number of ions per bunch (increasing grid size), as presented in Fig. 7.

The reported experiments show how the cells 'integrate' the nm and (sub-) μm DNA damage patterns. Apart from the very first single datum comparing focused protons and single carbon ions on a 5.4 μm grid [12], to our knowledge the present data provide the first direct experimental demonstration of the role in dicentrics formation on the (sub-) micrometer clustering of DNA damage. Studies will be reported elsewhere on how this sub-micrometer focusing affects other biological endpoints, especially cell survival, serving as a hitherto unprecedented benchmark of amorphous track structure models such as the local effect model used in carbon ion radiotherapy [25].

The reported PARTRAC simulations of the dicentrics experiments are based on an *ad hoc* A_L nucleus model that consists of the 22 largest human chromosomes, using the geometry as in lymphocytes (spherical nucleus with 10 μm diameter). Omitting the smallest 24 human chromosomes leads to a structure with additional unoccupied regions compared to standard model nuclei. The DNA content of this A_L nucleus model is about 4.2 Gbp, approximately 76% of the estimated DNA content of A_L cells: 5.4 Gbp for

Please cite this article in press as: T.E. Schmid, et al., Sub-micrometer 20 MeV protons or 45 MeV lithium spot irradiation enhances yields of dicentric chromosomes due to clustering of DNA double-strand breaks, Mutat. Res.: Genet. Toxicol. Environ. Mutagen. (2015), http://dx.doi.org/10.1016/j.mrgentox.2015.07.015

CHO-K1 cells [26] plus 0.135 Gbp for human chromosome 11 [27]. DSB repair capacity and kinetics in A_L cells may differ a lot from human cells, but detailed data on these issues are missing. Hence, model parameters describing DSB repair kinetics and DNA end mobility used in this work have been taken from model adaptation to human fibroblast data [14].

The resulting model predictions systematically overestimate the observed yields of dicentrics. This is not surprising, as dicentrics have been assessed experimentally in the first mitosis post irradiation, and especially most heavily damaged cells might have died out or not pursued their cycle up to mitosis within the given time frame, so that some dicentrics might have been missed by the given method. The simulations also overestimate the effect of proton focusing in intermediate regions studied here, and yield a decreasing trend with increasing focusing for lithium ions, contrary to the data. Note that in view of the aforementioned differences between modelled and real cells, the agreement of the simulations with the data cannot be judged too strictly. Nevertheless, to test the effect of varying model assumptions and the robustness of the predictions, a number of additional simulations have been performed. Test simulations with the full set of 46 human chromosomes (6.6 Gbp DNA content of the model lymphocyte nucleus) have not qualitatively changed the results presented here but provided about three-fold higher absolute yields of dicentrics; the effect of altered chromosome number was more pronounced than that of increased DNA content. The model lymphocyte has also a somewhat smaller nucleus (10 μm diameter) than the A_L cells (116 μm^2 determined from microscopy images). To test the role of nucleus size, simulations for lymphocytes have been compared to those for human fibroblasts with ellipsoidal shape ($10 \times 20 \times 5\ \mu m^3$); however, the main results have not changed qualitatively. Finally, a number of simulations with altered DSB repair parameters have been performed, keeping the limitation that the simulations reproduced typical DSB rejoining features such as biphasic kinetics with increasing role of the slow repair component for increasing LET and about 5% fraction of unrejoined breaks 1 day post irradiation [28]. Again, these altered DSB repair parameters have not changed the simulation results qualitatively.

This robustness of the model predictions may follow from the fact that the present PARTRAC repair model decides already at a very early repair stage on the DNA ends that will finally be ligated or may continue being attempted to be processed during the whole modelling period. Namely, as soon as two DNA ends form a synaptic complex, they are determined to get ligated or, rather rarely, stay within the process due to repair delay (steps 12–13 in Fig. 1), but there is no chance in the present scheme for the ends to separate and find other partners with which to join. Future work will be directed at testing whether altered assumptions on misrejoining events, e.g. allowing an exchange of DNA ends upon interaction of two synaptic complexes or break-up of synaptic complexes during the repair process, may modify the predictions qualitatively.

The experimentally observed yields of chromosome aberrations in total (including dicentrics, centric rings, and acentrics) are directly proportional to the yields of dicentrics (data not shown). Interestingly, total yields of inter-chromosomal exchange aberrations predicted by the reported PARTRAC simulations (Fig. 8) show trends that agree with the observed dicentrics (and total chromosome aberration) yields. Furthermore, preliminary data on dicentrics induced by single carbon ions on 5.4 μm and carbon ions focused to 7.6 and 10.6 μm grids show a decreasing trend with increasing grid size (data not shown). Taken together, these indications suggest that the model estimates on dicentrics might be revised, while the predictions on the overall induction of aberrations may well be more precise.

The experimental data indicate that sub-micrometer focusing affects not only the yields of dicentrics and tricentrics which are seen predominantly upon irradiation with lithium ions, but also their distribution among the irradiated cell population. Significantly overdispersed distributions of dicentrics are obtained for 45 MeV lithium ions at any of the four focusing degrees studied, as well as for highly focused 20 MeV protons. Quasi-homogeneous irradiation with protons, on the other hand, leads to regular dispersion, indicating Poisson distribution of dicentrics. Although intercellular distributions of dicentrics could be extracted also from the simulations, this issue has not been evaluated in this work.

The yields of dicentric chromosomes increase by focusing up to a factor of 2 for protons and 3 for lithium ions, respectively, compared to quasi-homogeneous irradiation, i.e. irradiation with single particles on a regular grid (0.5 μm for protons or 2.3 μm for lithium ions, respectively). The focusing enhances the RBE relative to 70 kV X-rays from 1.33 for quasi-homogeneous protons to 2.60 for those focused on the 10.6 μm grid, and from 2.11 for quasi-homogeneous lithium ions to 3.24 for the ones with the highest degree of focusing (Table 3). Note that this RBE of 3.24 for dicentrics induction by Li ions on the 10.6 μm grid is identical with that of single carbon ions on the 5.4 μm grid.

The present data have been gathered and simulations performed with A_L human-hamster hybrid cells. Additional experiments with human fibroblasts are planned to explicitly verify that the reported findings can be generalized for different cell types.

5. Conclusion

Conventional experiments on radiobiological effects of radiation types differing in their LET cannot separate the influence of micrometer scale DSB clustering from the inherently interlinked clustering on nanometer scale relevant for DSB induction. Submicrometer focusing of proton or lithium ions enables separating these scales. Total DSB yields are not altered but remain constant, characteristic of the given particle type. The focusing modifies the spatial distribution of DSB on the (sub-) micrometer scale. The reported data provide direct experimental demonstration that both scales are relevant for the induction of dicentrics. The reported study improves the understanding of the mechanisms by which radiation induces these lethal chromosome aberrations, and indicates the need for refining some of the assumptions on DSB repair and dicentrics formation in the PARTRAC biophysical modelling suite. More generally, such studies may have implications for radiotherapy with high-LET radiation regarding RBE. In particular, these results indicate that significant variations in RBE can be expected if low-, medium- or high-LET particles are applied in a spatially correlated manner.

Conflict of interests

The author declares that there is no conflict of interests.

Acknowledgements

Supported by the project 'LET-Verbund' (funding no. 02NUK031A, 02NUK031B and 02NUK031C) of the German Federal Ministry of Education and Research, by the DFG-Cluster of Excellence 'Munich-Centre for Advanced Photonics', by the DFG INST 95/980-1 FUGG, by the Helmholtz Zentrum Munich, and by the Maier Leibnitz Laboratory Munich. Discussions with Drs. M. Scholz and T. Friedrich (GSI Helmholtzzentrum für Schwerionenforschung Darmstadt, Germany) are gratefully acknowledged.

References

[1] M. Durante, J.S. Bedford, D.J. Chen, S. Conrad, M.N. Cornforth, A.T. Natarajan, D.C. van Gent, G. Obe, From DNA damage to chromosome aberrations: joining the break, Mutat. Res. 756 (2013) 5–13.

[2] M.N. Cornforth, J.S. Bedford, A quantitative comparison of potentially lethal damage repair and the rejoining of interphase chromosome breaks in low passage normal human fibroblasts, Radiat. Res. 111 (1987) 385–405.
[3] R.K. Sachs, P. Hahnfeld, D.J. Brenner, The link between low-LET dose-response relations and the underlying kinetics of damage production/repair/misrepair, Int. J. Radiat. Biol. 72 (1997) 351–374.
[4] K.K. Khanna, S.P. Jackson, DNA double-strand breaks: signaling: repair and the cancer connection, Nat. Genet. 27 (2001) 247–254.
[5] M.S. Kreipl, W. Friedland, H.G. Paretzke, Interaction of ion tracks in spatial and temporal proximity, Radiat. Environ. Biophys. 48 (2009) 349–359.
[6] T.E. Schmid, G. Dollinger, V. Hable, C. Greubel, O. Zlobinskaya, D. Michalski, S. Auer, A.A. Friedl, E. Schmid, M. Molls, B. Röper, The effectiveness of 20 MeV protons at nanosecond pulse lengths in producing chromosome aberrations in human-hamster hybrid cells, Radiat. Res. 175 (2011) 719–727.
[7] T.E. Schmid, G. Dollinger, V. Hable, C. Greubel, O. Zlobinskaya, D. Michalski, M. Molls, B. Röper, Relative biological effectiveness of pulsed and continuous 20 MeV protons for micronucleus induction in 3D human reconstructed skin tissue, Radiother. Oncol. 95 (2010) 66–72.
[8] T.E. Schmid, G. Dollinger, A. Hauptner, V. Hable, C. Greubel, S. Auer, A.A. Friedl, M. Molls, B. Röper, No evidence for a different RBE between pulsed and continuous 20 MeV protons, Radiat. Res. 172 (2009) 567–574.
[9] O. Zlobinskaya, C. Siebenwirth, C. Greubel, V. Hable, R. Hertenberger, N. Humble, S. Reinhardt, D. Michalski, B. Roper, G. Multhoff, G. Dollinger, J.J. Wilkens, T.E. Schmid, The effects of ultra-high dose rate proton irradiation on growth delay in the treatment of human tumor xenografts in nude mice, Radiat. Res. 181 (2014) 177–183.
[10] C. Greubel, W. Assmann, C. Burgdorf, G. Dollinger, G. Du, V. Hable, A. Hapfelmeier, R. Hertenberger, P. Kneschaurek, D. Michalski, M. Molls, S. Reinhardt, B. Röper, S. Schell, T.E. Schmid, C. Siebenwirth, T. Wenzl, O. Zlobinskaya, J.J. Wilkens, Scanning irradiation device for mice in vivo with pulsed and continuous proton beams, Radiat. Environ. Biophys. 50 (2011) 339–344.
[11] H. Rossi, Biophysical studies with spatially correlated ions: 1. background and theoretical considerations, Radiat. Res. 78 (1979) 185–191.
[12] T.E. Schmid, C. Greubel, V. Hable, O. Zlobinskaya, D. Michalski, S. Girst, C. Siebenwirth, E. Schmid, M. Molls, G. Multhoff, G. Dollinger, Low LET protons focused to submicrometershows enhanced radiobiological effectiveness, Phys. Med. Biol. 57 (2012) 5889–5907.
[13] W. Friedland, M. Dingfelder, P. Kundrat, P. Jacob, Track structures, DNA targets and radiation effects in the biophysical Monte Carlo simulation code PARTRAC, Mutat. Res. 711 (2011) 28–40.
[14] W. Friedland, P. Kundrat, Track structure based modelling of chromosome aberrations after photon and alpha-particle irradiation, Mutat. Res. 756 (2013) 213–223.
[15] D. Alloni, A. Campa, W. Friedland, L. Mariotti, A. Ottolenghi, Integration of Monte Carlo simulations with PFGE experimental data yields constant RBE of 2. 3 for DNA double-strand break induction by nitrogen ions between 125 and 225 keV/μm LET, Radiat. Res. 179 (2013) 690–697.
[16] W. Friedland, P. Jacob, P. Kundrat, Stochastic simulation of DNA double-strand break repair by non-homologous end joining based on track structure calculations, Radiat. Res. 173 (2010) 677–688.
[17] W. Friedland, P. Jacob, P. Kundrat, Mechanistic simulation of radiation damage to DNA and its repair: on the track towards systems radiation biology modelling, Radiat. Prot. Dosim. 143 (2011) 542–548.
[18] W. Friedland, P. Kundrat, E. Schmitt, Modelling proton bunches focused to submicrometre scales: low-LET radiation damage in high-LET-like spatial structure, Radiat. Prot. Dosim. (2015), http://dx.doi.org/10.1093/rpd/ncv146 (in press).
[19] A. Hauptner, R. Krucken, C. Greubel, V. Hable, G. Dollinger, G.A. Drexler, M. Deutsch, R. Lowe, A.A. Friedl, S. Dietzel, H. Strickfaden, T. Cremer, DNA-repair protein distribution along the tracks of energetic ions, Radiat. Prot. Dosim. 122 (2006) 147–149.
[20] A. Hauptner, S. Dietzel, G.A. Drexler, P. Reichart, R. Krucken, T. Cremer, A.A. Friedl, G. Dollinger, Microirradiation of cells with energetic heavy ions, Radiat. Environ. Biophys. 42 (2004) 237–245.
[21] C. Greubel, V. Hable, G.A. Drexler, A. Hauptner, S. Dietzel, H. Strickfaden, I. Baur, R. Krucken, T. Cremer, A.A. Friedl, G. Dollinger, Quantitative analysis of DNA-damage response factors after sequential ion microirradiation, Radiat. Environ. Biophys. 47 (2008) 415–422.
[22] J.F. Ziegler, M.D. Ziegler, J.P. Biersack, SRIM – The stopping and range of ions in matter, Nucl. Instrum. Methods Phys. Res. Sect. B 268 (2010) 1818–1823.
[23] IAEA, Cytogenetic analysis for radiation dose assessment. Technical Report Series 405 (2001).
[24] E. Schmid, H. Braselmann, U. Nahrstedt, Comparison of gamma-ray induced dicentric yields in human lymphocytes measured by conventional analysis and FISH, Mutat. Res. 348 (1995) 125–130.
[25] T. Friedrich, U. Scholz, T. Elsasser, M. Durante, M. Scholz, Calculation of the biological effects of ion beams based on the microscopic spatial damage distribution pattern, Int. J. Radiat. Biol. 88 (2012) 103–107.
[26] N.E. Lewis, X. Liu, Y. Li, H. Nagarajan, G. Yerganian, E. O'Brien, A. Bordbar, A.M. Roth, J. Rosenbloom, C. Bian, M. Xie, W. Chen, N. Li, D. Baycin-Hizal, H. Latif, J. Forster, M.J. Betenbaugh, I. Famili, X. Xu, J. Wang, B.O. Palsson, Genomic landscapes of Chinese hamster ovary cell lines as revealed by the *Cricetulus griseus* draft genome, Nat. Biotechnol. 31 (2013) 759–765.
[27] T.D. Taylor, H. Noguchi, Y. Totoki, A. Toyoda, Y. Kuroki, K. Dewar, C. Lloyd, T. Itoh, T. Takeda, W. Kim, X. She, K.F. Barlow, T. Bloom, E. Bruford, J.L. Chang, C.A. Cuomo, E. Eichler, M.G. FitzGerald, D.B. Jaffe, K. LaButti, R. Nicol, H.S. Park, C. Seaman, C. Sougnez, X. Yang, A.R. Zimmer, M.C. Zody, B.W. Birren, C. Nusbaum, A. Fujiyama, M. Hattori, J. Rogers, E.S. Lander, Y. Sakaki, Human chromosome 11 DNA sequence and analysis including novel gene identification, Nature 440 (2006) 497–500.
[28] E. Stenerlow, Hoglund, J. Carlsson, E. Blomquist, Rejoining of DNA fragments produced by radiations of different linear energy transfer, Int. J. Radiat. Biol. 76 (2000) 549–557.

Please cite this article in press as: T.E. Schmid, et al., Sub-micrometer 20 MeV protons or 45 MeV lithium spot irradiation enhances yields of dicentric chromosomes due to clustering of DNA double-strand breaks, Mutat. Res.: Genet. Toxicol. Environ. Mutagen. (2015), http://dx.doi.org/10.1016/j.mrgentox.2015.07.015